Clin Exp Metastasis (2009) 26:345–355
DOI 10.1007/s10585-008-9205-z

RESEARCH PAPER

# Imaging cancer dynamics in vivo at the tumor and cellular level with fluorescent proteins

**Robert M. Hoffman**

Received: 19 December 2007 / Accepted: 3 August 2008 / Published online: 12 September 2008


**Abstract** Whole-body imaging with fluorescent proteins has been shown to be a powerful technology to follow the dynamics of metastatic cancer. Whole-body imaging of fluorescent protein-expressing-cancer cells enables the facile determination of efficacy of candidate anti-tumor and anti-metastatic agents in mouse models. GFP-expressing transgenic mice transplanted with the RFP-expressing cancer cells enable the distinction of cancer and host cells and the efficacy of drugs on each type of cell. This is particularly useful for imaging tumor angiogenesis. Cancer-cell trafficking through the cardiovascular and lymphatic systems is the critical means of spread of cancer. The use of fluorescent proteins to differentially label cancer calls in the nucleus and cytoplasm and high-powered imaging technology are used to visualize the nuclear-cytoplasmic dynamics of cancer-cell trafficking in both blood vessels and lymphatic vessels in the live animal. This technology has furthered our understanding of the spread of cancer at the subcellular level in the live mouse. Fluorescent proteins thus enable both macro and micro imaging technology and thereby provide the basis for the new field of in vivo cell biology.

**Keywords** GFP · RFP · Cell invasion · Extravasation · Fluorescence imaging

R. M. Hoffman (✉)
AntiCancer, Inc., 7917 Ostrow Street, San Diego, CA 92111-3604, USA
e-mail: all@anticancer.com

R. M. Hoffman
Department of Surgery, University of California at San Diego, 200 West Arbor Drive, San Diego, CA 92103-8220, USA

## Background of in vivo imaging with fluorescent proteins

### Fluorescent proteins for in vivo imaging

To image and follow the dynamic natural course of cancer, a strong signal and high resolution are necessary. The *GFP* gene, cloned from the bioluminescent jellyfish *Aequorea victoria* [1], was chosen to satisfy these conditions because it has great potential for use as a cellular marker [2, 3]. GFP cDNA encodes a 283-amino acid monomeric polypeptide with Mr 27,000 [4, 5] that requires no other *A. victoria* proteins, substrates, or cofactors to fluoresce [6]. Gain-of-function bright mutants expressing the *GFP* gene have been generated by various techniques [7–9] and have been humanized for high expression and signal [10].

Red fluorescent proteins (RFP) from the *Discosoma* coral and other organisms have similar features as well as the advantage of longer-wavelength emission [11–13]. Red-emitting fluorescent proteins were first described in the late 1990s. The first such protein was isolated and cloned from the coral *Discosoma* sp. obtained from an aquarium shop in Moscow [14] and termed Ds-Red. After extensive modification by mutagenesis, a very bright red protein was eventually isolated, termed DsRed-2 with an emission wavelength peak of 588. DsRed-2 has shown to be very enabling for whole-body imaging. It has been used to non-invasively follow cancer metastasis in real time [15] in nude mice as well as whole-body image dual-color models of tumors expressing DsRed-2 growing in transgenic GFP nude mice as hosts [16]. In 2004, a report appeared [17] describing a series of red-shifted proteins obtained by mutating DsRed. These proteins, termed mCherry, mRaspberry, mPlum, and mTomato, had emission maxima as long as 649 nm. However, these mutants have low quantum

yields, thereby reducing their brightness. A very bright, red-shifted variant has now been isolated with an excitation peak at 588 mm emission peak at 635 nm both of which are relatively non-absorbed by issues and hemoglobin. After four cycles of random mutagenesis and further selection for bright, far-red-shifted proteins, Katushka was isolated. Katushka has many favorable properties in addition to its absorption and emission peaks including a rapid maturation time of 20 min. Importantly, an extinction coefficient of 65,000 $M^{-1}$ $cm^{-1}$ and quantum yield of 0.34, make Katushka the brightest fluorescent protein with an emission maximum beyond 620 nm. In cells, Katushka demonstrated no visible aggregates or other toxic effects [18].

Fluorescent mouse models

Transgenic mice ubiquitously expressing GFP were developed by Okabe's group [19]. Our laboratory crossed this strain with nude mice to obtain nude mice ubiquitously expressing GFP [16, 20]. Transgenic mice ubiquitously expressing RFP were originally developed by Nagy's group [21]. We crossed this mouse with nude mice to obtain nude mice ubiquitously expressing RFP [22, 23]. These colored mice are particularly useful for studying tumor-host interaction by transplanting tumor cells of different colors to these mice as discussed below.

The beginning of in vivo imaging with fluorescent proteins

Our laboratory pioneered the use of fluorescent protein for in vivo imaging [24] including non-invasive whole-body imaging [25]. These early studies demonstrated the power of fluorescent proteins for imaging tumor and metastasis noninvasively including possibilities to observe single cancer cells in the open mouse [24]. The first use of GFP to visualize cancer cells in vivo was by Chishima et al. [24] in our laboratory. Tumor cells were stably transfected with GFP and transplanted into several mouse models, including orthotopic models that have a high metastatic capacity. They showed that in excised live tissue, with no additional preparation, metastases could be observed in any organ at the single-cell level. In addition, cells were visualized in the process of intravasation and extravasation. The visualization of single metastatic cells in tissue is beyond the capabilities of standard histological techniques and so such ex vivo studies enabled, for the first time, micrometastases (including dormant cells) to be visualized in unfixed or unprocessed tissue.

## Imaging the primary tumor

Fluorescent proteins can be used to visualize any type of cancer process, including primary tumor growth.

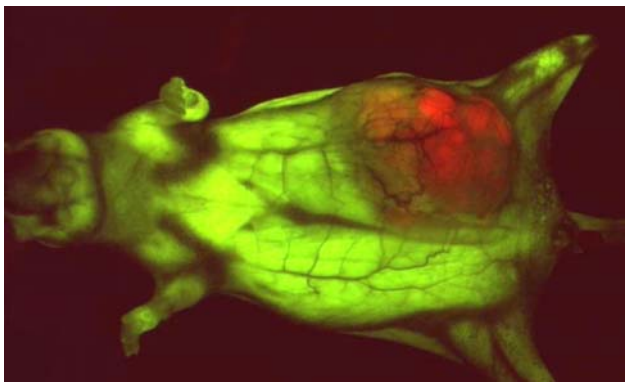

**Fig. 1** Whole-body image of orthotopically growing HCT 116-RFP human colon cancer in GFP nude mouse. Image was acquired in a fluorescence light box with a CCD camera 10 weeks after orthotopic implantation of HCT116-RFP cells [16]

Fluorescent proteins of many different colors have now been characterized, and these can be used to color-code cancer cells of a specific genotype or phenotype. For example, the behavior of highly metastatic cancer cells labeled with GFP and low metastatic cancer cells labeled with RFP can be directly compared in vivo. Alternatively, the host and the tumor can be differentially labeled with fluorescent proteins—a transgenic mouse expressing GFP in all of its cells (or in specific cells such as endothelial cells) transplanted with cancer cells expressing RFP enables the interaction between the cancer cells and the host cells to be visualized in real time (Fig. 1).

The fact that the excitation wavelengths for some fluorescent proteins are long enables real-time imaging to take place without harming the animals' tissues. Longer wavelength light causes few damaging events to proteins and DNA because of its lower energy. The long wavelength excitation of fluorescent proteins also reduces the extent of photobleaching compared with dyes that have a shorter wavelength excitation. Therefore, real-time tracking of tumor growth and metastasis can be carried out in the intact animal. Real-time imaging with fluorescent proteins is especially important when evaluating the efficacy of therapeutics.

Whole-body imaging with fluorescent proteins depends in large part on the brightness of the protein. Interference by skin autofluorescence is kept to a minimum with the use of proper filters. Very simple equipment such as an LED flashlight with a narrow-band filter and a bandpass emission filter can be used to whole-body image mice implanted with cells expressing fluorescent proteins [26].

Whole-body imaging is more effective when the fluorescent protein emits at longer wavelengths which are absorbed less by tissues and by physiological molecules such as hemoglobin and are also less scattered [27].

## Imaging the tumor microenvironment

### *Labeling of cancer cells with GFP in the nucleus and RFP in the cytoplasm to image nuclear-cytoplasmic dynamics and distinguish them from GFP or RFP colored stromal cells*

We have engineered dual-color fluorescent cells with one color in the nucleus and the other in the cytoplasm that enable real-time nuclear-cytoplasmic dynamics to be visualized in living cells in vivo as well as in vitro. To obtain the dual-color cells, RFP was expressed in the cytoplasm of the cancer cells, and GFP linked to histone H2B was expressed in the nucleus. Nuclear GFP expression enabled visualization of nuclear dynamics, whereas simultaneous cytoplasmic RFP expression enabled visualization of nuclear cytoplasmic ratios as well as simultaneous cell and nuclear shape changes. Thus, total cellular dynamics can be visualized in the living dual-color cells in real time [28].

To noninvasively visualize cellular and subcellular events in the tumor microenvironment in real time in the live mouse, we used the Olympus IV100 laser scanning microscope with a 1.3-mm-diameter stick objective that is up to 2 cm in length. The system allows an imaging depth that extends to at least 200 μm. This novel imaging system, coupled with the use of the cancer cells labeled in the nucleus with GFP and RFP in the cytoplasm and a transgenic GFP or RFP mouse as the host, has enabled noninvasive in vivo imaging of the cancer and stromal cells in the tumor microenvironment at the subcellular level. Three-color whole-body imaging of the two-color cancer cells interacting with the GFP-expressing stromal cells was carried out. In this model, drug response of both cancer and stromal cells in the intact live animal was also imaged in real time. Various in vivo phenomena of tumor–host interaction and cellular dynamics were imaged, including mitotic and apoptotic cancer cells, stromal cells intimately interacting with the cancer cells, tumor vasculature, and tumor blood flow. This new model system enabled the first cellular and subcellular images of unperturbed tumors in the live intact animal. New visible real-time targets for novel anticancer agents are provided in this model, including the color-coded interacting cancer and stromal cells, tumor vasculature, and blood flow. This imageable model should lead to many new insights of the tumor microenvironment [29] (Fig. 2). For example, Weinberg et al. [30], using GFP tumor cells, have shown that what are called mesenchymal stem cells may localize in tumor stroma and promote metastasis. Unfortunately, this study was conducted in a subcutaneously-growing tumor rather than an orthotopic tumor, where the tumor microenvironment is relevant.

## Imaging the metastatic process

### *Imaging angiogenesis and cancer-cell trafficking*

High-resolution intravital video microscopy of GFP-expressing tumor cells provides a powerful tool for directly observing steps in the metastatic process. Individual, non-dividing cells as well as micro- and macrometastases can be clearly visualized and quantified. Cellular details, such as pseudopodial projections, can be clearly seen [31]. Farina et al. [32] observed tumor cell motility at the single-cell level, including movement in and out of blood vessels, using GFP-expressing cells. Condeelis et al. [33] have used GFP imaging to view cells in time-lapse images in a single optical section using a confocal microscope. The polarity of tumor cells, along with their response to chemotatic cytokines, has been visualized by intra-vital imaging [32]. Condeelis et al. [34] have shown with multiphoton microscopy that tumor cell intravasation occurs in association with perivascular macrophages in mammary tumors. These techniques enable a greater understanding of tumor cell migration in vivo.

The dynamics of blood-vessel recruitment by cancer cells was investigated by Amoh et al. [35]. They used transgenic mice expressing GFP under the control of a neural-stem-cell marker nestin. The nestin-promoter-driven GFP (ND-GFP) has shown that nestin is expressed in hair-follicle stem cells and the blood vessel network interconnecting hair follicles in the skin. The hair follicles were shown to directly give rise to the nestin-expressing blood vessels. Following transplantation of the RFP-expressing murine melanoma cell line B16F10 into these animals, tumor angiogenesis was visualized using dual-color fluorescence imaging. ND-GFP was expressed in the proliferating endothelial cells and nascent blood vessels in the growing tumor. Immunohistochemical staining showed that the endothelial-cell-specific antigen CD31 was expressed in ND-GFP-expressing nascent blood vessels, showing that the tumor directly recruited the nestin-expressing cells. Doxorubicin inhibited tumor angiogenesis as well as tumor growth in these mice [36].

Brown et al. [37] showed that multiphoton laser-scanning microscopy (MPLSM) [38] could provide high-resolution three-dimensional images of angiogenesis-associated gene expression and that this technique could be used to investigate deeper regions of GFP-expressing tumors in dorsal skin-fold chambers. MPLSM offers significant advantages over other visualization techniques, such as improved signal/background ratios and longer sample lifetimes, as well as greater imaging depths. Overall, these advantages enable visualization of tumors in situ at the cellular level of resolution [31, 32]. To understand another aspect of angiogenesis, Fukumura et al. [39, 40] monitored the activity of

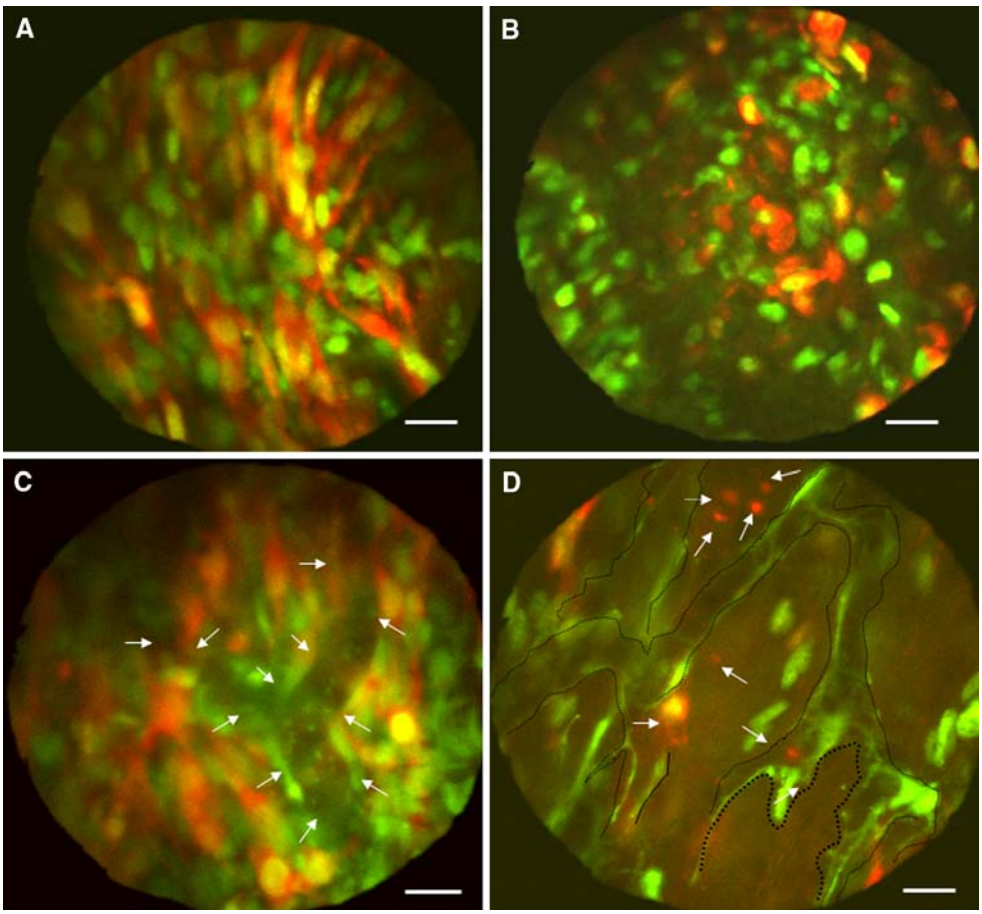


**Fig. 2** Noninvasive, subcellular imaging of drug response of dual-color mouse mammary cancer cells and GFP stromal cells. MMT-GFP-RFP cells were injected in the footpad of GFP transgenic nude mice. (**a**) Noninvasive image of untreated MMT-GFP-RFP cells in the footpad of a live GFP mouse. Note the numerous spindle-shaped MMT-GFP-RFP cells interdispersed among the GFP host cells. (**b**) Noninvasive image of MMT-GFP-RFP cancer cells in a live GFP nude mouse 12 h after treatment with doxorubicin (10 mg/kg). The cancer cells lost their spindle shape, and the nuclei appear contracted. (**c**) Noninvasive image of MMT-GFP-RFP tumor. Numerous spindle-shaped MMT-GFP-RFP cells interacted with GFP-expressing host cells. Well-developed tumor blood vessels and real-time blood flow were visualized by whole-body imaging (arrows). (**d**) Noninvasive imaging of in vivo drug response of MMT-GFP-RFP cancer cells and GFP stromal cells 12 h after i.v. injection of 10 mg/kg doxorubicin. All of the visible MMT-GFP-RFP cells lost their spindle shape. Many of the cancer cells fragmented (arrows). Tumor blood vessels were damaged (dashed black lines), and the number of cancer cells was dramatically reduced 12 h after chemotherapy. Bar = 20 μm [30]

the vascular endothelial growth factor (VEGF) promoter in transgenic mice that expressed GFP under the control of the VEGF promoter. MPLSM showed that the tumor was able to induce activity of the VEGF promoter and subsequent blood-vessel formation.

## Imaging nuclear and cytoplasmic deformation of trafficking cancer cells

Chishima et al. [24] and Huang et al. [41] showed that GFP-transduced cancer cells allowed the imaging of tumor cells in blood vessels. To examine cell behavior during intravasation, Wyckoff et al. [42] have used GFP imaging to view these cells in time-lapse images within a single optical section using a confocal microscope. In vivo imaging of the primary tumors indicated that both metastatic and nonmetastatic cells are motile and show protrusive activity. Metastatic cells show greater orientation toward blood vessels. Nonmetastatic cells fragment when interacting with vessels.

Cancer cells that escape from the primary site into the blood circulation eventually flow to the capillaries of the organs of the body [43]. In vivo video microscopy has shown that both lung and liver capillaries are very efficient at arresting the flow of cancer cells. Most circulating cancer cells arrest by size restriction. Capillaries are small, typically 3–8 μm in diameter. Capillaries allow the passage of RBC which average 7 μm in diameter and are highly deformable [43]. However, many cancer cells are large being 20 μm or more in diameter. Flow or arrest in

capillaries is determined by physical factors, such as the relative sizes of the cells and the capillaries, the blood pressure in the organ and the deformability of the cell [43]. Cancer cells can, under certain conditions, undergo adhesive arrest in the capillary vessels that are larger than the cell diameter.

The ability to image nuclear-cytoplamic dynamics in vivo is a major advance in our ability to understand the proliferation, quiescence, dormancy, trafficking, and death of cancer cells in the living animal. With this powerful technology, we will be able to visualize in vivo the most fundamental properties of cancer, including the reversible transition between cancer-cell proliferation and quiescence, how prolonged quiescence may lead to dormancy, the dynamics of cell death and the nuclear-cytoplasmic dynamics of cancer-cell spread. Most importantly, we will have an opportunity to visualize, in real time in the live animal, the activity of novel drugs on these processes as well as how drugs induce cell death at the subcellular level. With this technology, we can expect to discover new classes of drugs for cancer.

*Imaging nuclear-cytoplasmic dynamics of trafficking and extravasating cancer cells in real time*

We have described real-time imaging of the deformation of cancer cells and their nuclei in vivo. In addition to the deformability, we imaged migration of HT-1080-dual-color cells in microvessels and capillaries in real time. The capability to make such measurements in vivo should enable better understanding of the mechanism of metastasis [44]. Immediately after the dual-color cells were injected in the heart of nude mice, a skin flap on the abdomen was made. With a color CCD camera, we could observe highly elongated cancer cells and nuclei in capillaries in the skin flap in living mice. The migration velocities of the cancer cells in the capillaries were measured by capturing images of the dual-color fluorescent cells over time. The cells and nuclei in the capillaries elongated to fit the width of these vessels. The average length of the major axis of the cancer cells in the capillaries increased to approximately four times their normal length. The nuclei increased their length 1.6 times in the capillaries. Cancer cells in capillaries over 8 μm in diameter could migrate up to 48.3 μm/h. The data suggests that the minimum diameter of capillaries where cancer cells are able to migrate is approximately 8 μm. The use of the dual-color cancer cells differentially labeled in the cytoplasm and nucleus and associated fluorescent imaging provide a powerful tool to understand the mechanism of cancer cell migration and deformation in small vessels [44] (Fig. 3).

Dual-color cancer cells were injected by a vascular route in an abdominal skin flap in nude mice. The Olympus OV100 has four objective lenses, parcentered and parfocal, enabling imaging from macrocellular to subcellular. We observed the nuclear and cytoplasmic behavior of cancer

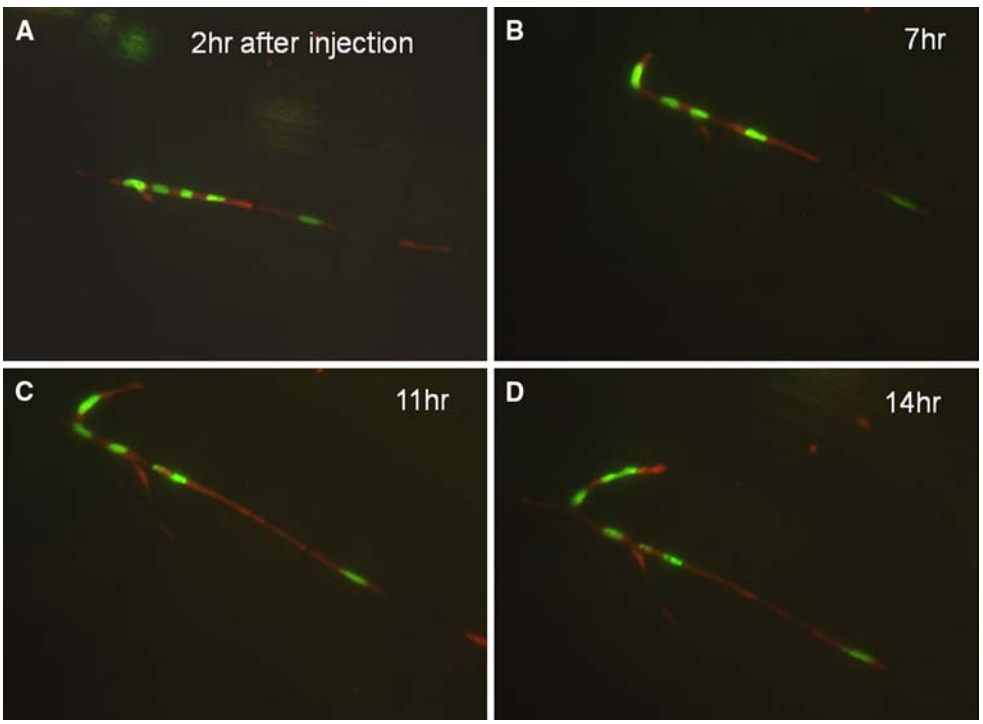


**Fig. 3** Migration velocity of HT-1080-dual-color cells in capillaries. (**a**–**d**) Migration of cells in capillaries from 2 to 14 h. Bar = 50 μm [44]

cells in real time in blood vessels as they moved by various means or adhered to the vessel surface in the abdominal skin flap. Some of the cancer cells died in the blood vessels by a process termed clasmocytosis, the separation of nucleus and cytoplasm. During extravasation, real-time dual-color imaging showed that cytoplasmic processes of the cancer cells exited the vessels first, with nuclei following along the cytoplasmic projections. Both cytoplasm and nuclei underwent deformation during extravasation. Different cancer cell lines seemed to strongly vary in their ability to extravasate. With the dual-color cancer cells and the highly sensitive whole-mouse imaging system described here, the subcellular dynamics of cancer metastasis can now be observed in live mice in real time [45].

*Imaging trafficking of cancer cells in lymphatic vessels*

The major pathways of cancer cell dissemination are the lymphatic system and the circulatory system. However, the role of the lymphatic system in cancer metastasis is less well understood compared with the circulatory system [46].

Lymphangiogenesis is associated with an increased incidence of lymph node metastasis. Tumor-secreted cytokines, such as vascular endothelial growth factor (VEGF)-C and VEGF-D, bind to VEGF receptors on lymphatic endothelial cells and induce proliferation of new lymphatic capillaries [47, 48]. However, despite its importance in lymphatic metastasis, cancer cell trafficking in lymphatic vessels, including entrance to the targeted lymph node, has been insufficiently investigated. Some studies suggest that the trafficking of tumor cells to lymph nodes resembles the normal migration of dendritic cells and that they follow a chemokine gradient [49]. Tumor cells that express certain types of chemokine receptors are more likely to metastasize to the lymph node. A promising approach to the further understanding of trafficking of cancer cells in lymphatics is imaging [50].

In a recent report [50], we demonstrated real-time imaging of cancer cell trafficking in lymphatic vessels. Cancer cells labeled with both GFP in the nucleus and RFP in the cytoplasm or with GFP only or RFP only were injected into the inguinal lymph node of nude mice. The labeled cancer cells trafficked through lymphatic vessels where they were imaged via a skin flap in real time at the cellular level until they entered the axillary lymph node. The bright fluorescence of the cancer cells and the real-time microscopic imaging capability of the Olympus OV100 small-animal imaging system enabled imaging of the trafficking cancer cells in the lymphatics. Using this imaging strategy, two different cancer cell lines, one expressing GFP and the other expressing RFP, were simultaneously injected in the inguinal lymph node. Fluorescence imaging readily distinguished the two color-coded cell lines and their different abilities to survive in the lymphatic system. Using this imaging technology, we also investigated the role of pressure on tumor-cell shedding into lymphatic vessels. Pressure was generated by placing 25- and 250-g weights for 10 s on the bottom surface of a tumor-bearing footpad. Tumor cell fragments, single cells, and emboli shed from the footpad tumor were easily distinguished with the labeled cells and OV100 imaging system. Increasing pressure on the tumor increased the numbers of shed cells, fragments, and emboli. Pressure also deformed the shed emboli, increasing their maximum major axis. Imaging lymphatic trafficking of cancer cells can reveal critical steps of lymph node metastasis.

Overall, these results show that the interaction of cancer cells with their vascular environment is complex. Cancer cells also seem to be highly motile and can significantly alter their shape to squeeze down narrow vessels. They can also form micrometastases inside larger vessels as well as become intimately associated with the vessel wall. These visual findings are intriguing and indicate that we still have much to learn about the tumor–endothelial cell interaction process.

*Color-coding metastatic cells*

It is thought that metastases are clonal and originate from rare cells in primary tumors, which are genotypically and phenotypically heterogeneous. Studies using DNA microarray analyses challenge this hypothesis and indicate that the genetic background of the host is an important determinant of metastatic potential, implying that metastases are not necessarily clonal. Previous methods of determining the clonality of metastases used complicated karyotype or molecular analyses, thereby limiting the number of metastatic colonies analyzed and the conclusions that could be drawn. Yamamoto et al. [51] described the use of GFP-labeled or RFP-labeled HT-1080 human fibrosarcoma cells to determine clonality of individual metastases by simple fluorescence visualization of metastatic colonies after mixed implantation into severe combined immunodeficient (SCID) mice. The resulting pure red or pure green colonies were scored as clonal, whereas mixed red and green colonies were scored as non-clonal. Analysis of the resulting lung colonies showed that 95% were either pure green or pure red, indicating clonal origin, whereas 5% were composed of red and green cells, indicating non-clonal origin. The clonality of the lung metastases was found to be dependent on the number of cells injected.

Glinskii et al. [52] reported that GFP-expressing orthotopic human prostate carcinomas efficiently delivered viable metastatic cells to the host circulation. This is in contrast to the ectopic tumors of the same lineage, which do not deliver live cells into the circulation. Co-implantation of

an equivalent mixture of GFP-expressing human prostate tumor cells, previously isolated from the circulation, and parental RFP-expressing human prostate carcinoma cells into the prostate has shown that the GFP-labeled, previously circulating cells are more metastatic than the RFP-labeled parental cells. Berezovskaya et al. [53] subsequently demonstrated that the metastatic human prostate carcinoma cells selected for survival in the circulation have increased resistance to anoikis because of increased expression of the X-linked inhibitor of apoptosis protein (XIAP). Glinsky et al. [54] have subsequently shown that, when co-injected, the high and low metastatic cells can exchange genetic information and produce an even more metastatic cell line.

These techniques enable the visualization and distinction of tumor cell types that have different properties in the live animal. The color-coding techniques can also be applied to visualizing the action of specific genes on tumor growth and metastasis.

*Imaging dormant tumor cells*

In some instances, viable tumor cells are seen by fluorescent protein expression to lodge in the lung but not grow, a process termed dormancy that might be organ specific. Fluorescent protein imaging enables us to visualize whether a cell that reaches a distant organ will proliferate, arrest or die and to establish the factors that influence this process.

Large detectable metastases did not form after nude mice were given an intravenous injection of chromosome-6-transduced tumor cells expressing GFP [55]. However, fluorescence microscopy showed micrometastases (single cells or clusters of fewer than 10 cells) in the lungs, indicating that these cells were present but had failed to proliferate. When isolated from the lungs up to 60 days after the injection, these cells were able to grow in culture and formed tumors when injected into the skin; therefore, the cells were still viable but were dormant in the lung. This result implies that some genes on chromosome 6 interfere specifically with growth in the lung but not in the skin.

An isogenic pair of metastatic (M4A4) and non-metastatic (NM2C5), GFP-labeled human breast cancer cell lines derived from the same patient and inoculated into the mammary glands of nude mice were used to investigate the dissemination patterns and fate of cells that escaped spontaneously from the resulting tumors. After tumors appeared, single fluorescent tumor cells were regularly seen in the lungs, even in animals inoculated with NM2C5, which fail to form secondary tumors in other organs. The sensitivity of the technique confirmed the continuing presence of scattered NM2C5 cells in the lung after primary tumor resection, although they formed no metastases by 6 months. These self-disseminated human tumor cells were retrievable from the tissues and were still viable and malignant, manifested by indefinite proliferation in vitro and local tumorigenicity in vivo. Therefore, these scattered tumor cells were rendered indefinitely quiescent by the microenvironment of the lung tissue [56].

The capacity to see dormant tumor cells in vivo should enhance our understanding of dormant cells and might help us address why cancer patients can relapse many years after the eradication of the primary tumor. This is especially true for breast cancer patients.

*Imaging the response of metastasis to treatment*

The properties of fluorescent proteins that enable whole-body imaging in real time also mean that the efficacy of therapeutic anticancer treatments can be seen directly without the need for any invasive procedure in the tumor-bearing mouse. In effect, each animal serves as its own control when whole-body imaging is used to follow drug efficacy—a radical departure from sacrificing mice at each time point and comparing the results. Examples include the use of GFP- or RFP-expressing orthotopic metastatic models treated with candidate antimetastatic agents [15, 57] (Fig. 4). In addition, the response to surgical-resection followed by adjuvant treatment has been assessed by whole-body imaging of GFP- or RFP-expressing tumors [58].

Such techniques can also be used to analyse the effect of specific anticancer treatments on known genetic backgrounds. Fluorescent protein imaging, especially whole-body imaging, enables rapid analysis of the effects of single or multiple gene changes on cancer aggressiveness and drug sensitivity. Using a mouse model harboring primary, genetically modified MYC-driven lymphomas that express GFP, whole-body imaging showed that disruption of apoptosis downstream of p53 by BCL2 confers a highly aggressive tumor phenotype, which metastasizes throughout the mouse body [59]. Moreover, whole-body imaging shows that MYC-driven GFP-expressing lymphomas with p53 or INK4A and ARF mutations, or that overexpress BCL2, respond poorly to cyclophosphamide therapy in vivo compared with wild-type cells [60].

In addition to whole-body imaging techniques, other techniques can be used to visualize treatment response with fluorescent proteins such as intravital imaging [31] and confocal microscopy including dual-photon scanning-laser imaging systems [33, 37, 61] (Table 1).

These real-time fluorescent imaging techniques will increase our ability to discover new drugs and genes that mitigate cancer growth and progression. Moreover, such techniques enable visualization at what stage tumors become resistant to specific treatments and might highlight other ways to circumvent drug resistance.

**Table 1** Instrumentation for in vivo imaging with fluorescent proteins

| Step in tumor progression | Type of instrumentation | Reference |
|---|---|---|
| Primary tumor growth | LED and goggles | [26] |
| | FluorVivo (Indec Systems, Santa Clara, CA) | |
| | I-Box (UVP LLS, Upland, CA) | |
| | OV100 (Olympus Corp., Tokyo, Japan) | [45] |
| | IVIS (Caliper Life Sciences, Hopkinton, MA) | [64] |
| Macro-metastasis | LED and goggles | [26] |
| | FluorVivo (Indec Systems, Santa Clara, CA) | |
| | I-Box (UVP LLS, Upland, CA) | |
| | OV100 (Olympus Corp., Tokyo, Japan) | [45] |
| | IVIS (Caliper Life Sciences, Hopkinton, MA) | [64] |
| Micro-metastasis | OV100 (Olympus Corp., Tokyo, Japan) | [45] |
| | Multiphoton laser-scanning microscope (MPLSM) | [37] |
| | Spinning disk confocal microscope | [61] |
| | Bio-Rad Radiance 2000 multiphoton microscope | [34] |
| Hematogenous trafficking | OV100 (Olympus Corp., Tokyo, Japan). | [30] |
| | Multiphoton laser-scanning microscope (MPLSM) | [37] |
| | Spinning disk confocal microscope | [61] |
| | Bio-Rad Radiance 2000 multiphoton microscope | [34] |
| Intralymphatic trafficking | OV100 (Olympus Corp., Tokyo, Japan) | [45] |
| | Multiphoton laser-scanning microscope (MPLSM) | [37] |
| | Spinning disk confocal microscope | [61] |
| | Bio-Rad Radiance 2000 multiphoton microscope | [34] |
| Extravasation | OV100 (Olympus Corp., Tokyo, Japan) | [30] |
| | Multiphoton laser-scanning microscope (MPLSM) | [37] |
| | Spinning disk confocal microscope | [61] |
| | Bio-Rad Radiance 2000 multiphoton microscope | [34] |
| Tumor shedding | OV100 (Olympus Corp., Tokyo, Japan) | [45] |
| | Multiphoton laser-scanning microscope (MPLSM) | [37] |
| | Spinning disk confocal microscope | [61] |
| | Bio-Rad Radiance 2000 multiphoton microscope | [34] |
| Tumor angiogenesis | OV100 (Olympus Corp., Tokyo, Japan) | [45] |
| | Multiphoton laser-scanning microscope (MPLSM) | [37] |
| | Spinning disk confocal microscope | [61] |
| | Bio-Rad Radiance 2000 multiphoton microscope | [34] |
| Tumor microenvironment cellular interaction | OV100 (Olympus Corp., Tokyo, Japan) | [45] |
| | IV100 (Olympus Corp., Tokyo, Japan) | [30] |
| | Multiphoton laser-scanning microscope (MPLSM) | [37] |
| | Spinning disk confocal microscope | [61] |
| | Bio-Rad Radiance 2000 multiphoton microscope | [34] |
| Cancer cell-cycle events | OV100 (Olympus Corp., Tokyo, Japan) | [45] |
| | IV100 (Olympus Corp., Tokyo, Japan) | [30] |
| | Multiphoton laser-scanning microscope (MPLSM) | [37] |
| | Spinning disk confocal microscope | [61] |
| | Bio-Rad Radiance 2000 multiphoton microscope | [34] |
| Cancer cell apoptosis | OV100 (Olympus Corp., Tokyo, Japan) | [45] |
| | IV100 (Olympus Corp., Tokyo, Japan) | [30] |
| | Multiphoton laser-scanning microscope (MPLSM) | [37] |
| | Spinning disk confocal microscope | [61] |
| | Bio-Rad Radiance 2000 multiphoton microscope | [34] |

**Table 1** continued

| Step in tumor progression | Type of instrumentation | Reference |
|---|---|---|
| Cancer cell dormancy | OV100 (Olympus Corp., Tokyo, Japan) | [45] |
| | IV100 (Olympus Corp., Tokyo, Japan) | [30] |
| | Multiphoton laser-scanning microscope (MPLSM) | [37] |
| | Spinning disk confocal microscope | [61] |
| | Bio-Rad Radiance 2000 multiphoton microscope | [34] |
| Intravital cellular or subcellular | OV100 (Olympus Corp., Tokyo, Japan) | [45] |
| | IV100 (Olympus Corp., Tokyo, Japan) | |
| | Multiphoton laser-scanning microscope (MPLSM) | [37] |
| | Spinning disk confocal microscope | [61] |
| | Bio-Rad Radiance 2000 multiphoton microscope | [34] |
| Noninvasive cellular or subcellular | IV100 (Olympus Corp., Tokyo, Japan) | [30] |
| | Multiphoton laser-scanning microscope (MPLSM) | [37] |
| | Spinning disk confocal microscope | [61] |
| | Bio-Rad Radiance 2000 multiphoton microscope | [34] |

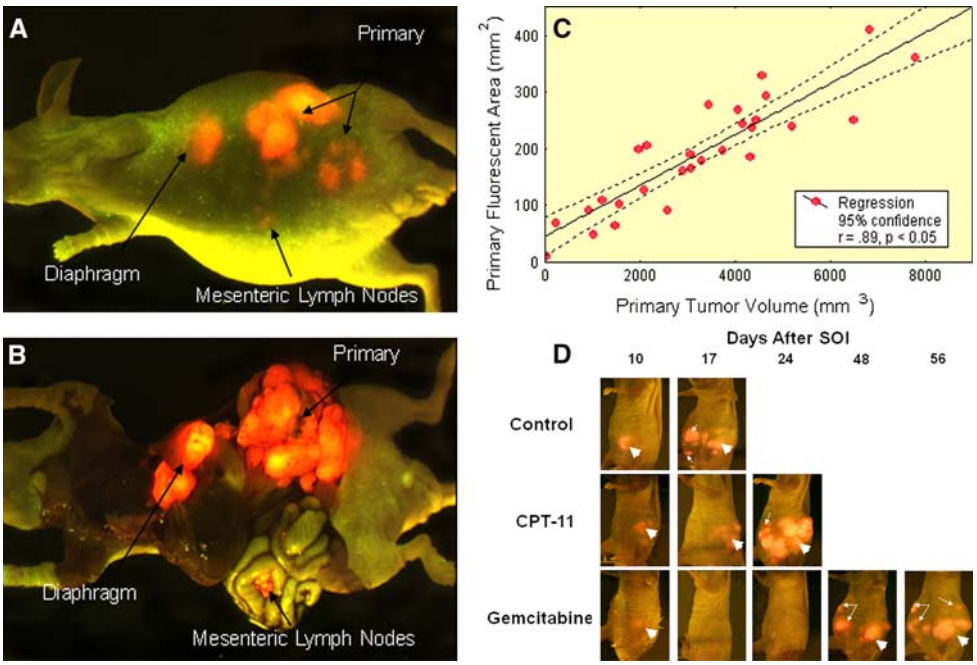


**Fig. 4** External versus internal quantitative imaging. (**a**) External and (**b**) open images of a single, representative, control mouse at autopsy on day 17 after surgical orthotopic implantation (SOI). Extensive locoregional and metastatic growth is visualized by selectively exciting DsRed2-expressed in the tumors. A strong correlation between the fluorescence visualized externally and that obtained after laparotomy is evident, despite the presence of intra-abdominal ascites. (**c**) Red fluorescent area quantified using external fluorescence imaging correlated strongly with tumor volume measured directly with calipers. At autopsy, measurement of externally visualized fluorescent area and direct measurements of the primary tumor of each mouse were obtained. Significant correlation ($r = 0.89$, $P < 0.05$) was observed between these values. (**d**) Real-time, in vivo imaging of MIA-PaCa-2-RFP pancreatic cancer progression and evaluation of therapeutic efficacy over time. Representative mice from each treatment group on days 10, 17, 24, 48, and 56 after tumor implantation are shown. Thick arrows show primary tumor, and thin arrows indicate metastatic tumor. CPT-11 suppressed primary and metastatic tumor growth compared with controls. In contrast, gemcitabine successfully induced temporary regression of disease over the first month, after which growth and distant metastasis of tumor accelerated despite continued treatment [15]

## Conclusions

Naturally fluorescent proteins have revolutionized biology by enabling what was formerly invisible to be seen clearly. These proteins have allowed us to visualize, in real time, cancer dynamics in living animals, including tumor growth, metastasis, cell mobility, invasion and angiogenesis. These multi-colored proteins have allowed the color-coding of cancer cells growing in vivo and enabled the distinction of host from tumor with single-cell resolution. Visualization

of many aspects of cancer initiation and progression in vivo are now possible, even at the subcellular level, with fluorescent proteins. Bright red-shifted proteins are being developed to enable deeper noninvasive imaging and overcoming limits of shorter wavelength proteins [22]. New applications such as linking different colored proteins to cell cycle specific proteins has now enabled imaging to distinguish where any cell is in the cell cycle [62]. Linking multiple fluorescent proteins of different colors in one vector with the genes separated by recombination sites has enabled development of transgenic mice with brain cells of approximately 100 different colors [63]. Application of this technology to cancer will enable the real-time imaging of 100 or more color-coded subclones in tumors during metastasis and should allow identification of metastatic stem cells. Important advances in our knowledge of the dynamic cell biology of cancer should be made with the imaging technology described in this review.

## References


1. Prasher DC, Eckenrode VK, Ward WW et al (1992) Primary structure of the *Aequorea victoria* green-fluorescent protein. Gene 111:229–233
2. Chalfie M, Tu Y, Euskirchen G et al (1994) Green fluorescent protein as a marker for gene expression. Science 263:802–805
3. Cheng L, Fu J, Tsukamoto A, Hawley RG (1996) Use of green fluorescent protein variants to monitor gene transfer and expression in mammalian cells. Nat Biotechnol 14:606–609
4. Cody CW, Prasher DC, Westler WM et al (1993) Chemical structure of the hexapeptide chromophore of the Aequorea green fluorescent protein. Biochemistry 32:1212–1218
5. Yang F, Moss LG, Phillips GN Jr (1996) The molecular structure of green fluorescent protein. Nat Biotechnol 14:1246–1251
6. Morin J, Hastings J (1971) Energy transfer in a bioluminescent system. J Cell Physiol 77:313–318
7. Cormack B, Valdivia R, Falkow S (1996) FACS-optimized mutants of the green fluorescent protein (GFP). Gene 173:33–38
8. Crameri A, Whitehorn EA, Tate E, Stemmer WP (1996) Improved green fluorescent protein by molecular evolution using DNA shuffling. Nat Biotechnol 14:315–319
9. Delagrave S, Hawtin RE, Silva CM et al (1995) Red-shifted excitation mutants of the green fluorescent protein. Biotechnology 13:151–154
10. Heim R, Cubitt AB, Tsien RY (1995) Improved green fluorescence. Nature 373:663–664
11. Zolotukhin S, Potter M, Hauswirth WW et al (1996) A 'humanized' green fluorescent protein cDNA adapted for high-level expression in mammalian cells. J Virol 70:4646–4654
12. Gross LA, Baird GS, Hoffman RC et al (2000) The structure of the chromophore within DsRed, a red fluorescent protein from coral. Proc Natl Acad Sci USA 97:11990–11995
13. Fradkov AF, Chen Y, Ding L et al (2000) Novel fluorescent protein from *Discosoma* coral and its mutants possesses a unique far-red fluorescence. FEBS Lett 479:127–130
14. Matz MV, Fradkov AF, Labas YA et al (1999) Fluorescent proteins from nonbioluminescent Anthozoa species. Nat Biotechnol 17:969–973
15. Katz MH, Takimoto S, Spivak D et al (2003) A novel red fluorescent protein orthotopic pancreatic cancer model for the preclinical evaluation of chemotherapeutics. J Surg Res 113:151–160
16. Yang M, Li L, Jiang P et al (2003) Dual-color fluorescence imaging distinguishes tumor cells from induced host angiogenic vessels and stromal cells. Proc Natl Acad Sci USA 100:14259–14262
17. Shaner NC, Campbell RE, Steinbach PA et al (2004) Improved monomeric red, orange and yellow fluorescent proteins derived from *Discosoma* sp. red fluorescent protein. Nat Biotechnol 22:1567–1572
18. Shcherbo D, Merzlyak EM, Chepurnykh TV et al (2007) Bright far-red fluorescent protein for whole-body imaging. Nat Methods 4:741–746
19. Okabe M, Ikawa M, Kominami K et al (1997) 'Green mice' as a source of ubiquitous green cells. FEBS Lett 407:313–319
20. Yang M, Reynoso J, Jiang P et al (2004) Transgenic nude mouse with ubiquitous green fluorescent protein expression as a host for human tumors. Cancer Res 64:8651–8656
21. Vintersten K, Monetti C, Gertsenstein M et al (2004) Mouse in red: red fluorescent protein expression in mouse ES cells, embryos, and adult animals. Genesis 40:241–246
22. Hoffman RM (2008) A better fluorescent protein for whole-body imaging. Trends Biotechnol 26:1–4
23. Hoffman RM (2008) Imaging in mice with fluorescent proteins: from macro to subcellular. Sensors 8:1157–1173
24. Chishima T, Miyagi Y, Wang X et al (1997) Cancer invasion and micrometastasis visualized in live tissue by green fluorescent protein expression. Cancer Res 57:2042–2047
25. Yang M, Baranov E, Jiang P et al (2000) Whole-body optical imaging of green fluorescent protein-expressing tumors and metastases. Proc Natl Acad Sci USA 97:1206–1211
26. Yang M, Luiken G, Baranov E et al (2005) Facile whole-body imaging of internal fluorescent tumors in mice with an LED flashlight. Biotechniques 39:170–172
27. Hoffman RM (2005) The multiple uses of fluorescent proteins to visualize cancer in vivo. Nat Rev Cancer 5:796–806
28. Yamamoto N, Jiang P, Yang M et al (2004) Cellular dynamics visualized in live cells in vitro and in vivo by differential dual-color nuclear-cytoplasmic fluorescent-protein expression. Cancer Res 64:4251–4256
29. Yang M, Jiang P, Hoffman RM (2007) Whole-body subcellular multicolor imaging of tumor-host interaction and drug response in real time. Cancer Res 67:5195–5200
30. Karnoub AE, Dash AB, Vo AP et al (2007) Mesenchymal stem cells within tumour stroma promote breast cancer metastasis. Nature 449:557–563
31. Naumov GN, Wilson SM, MacDonald IC et al (1999) Cellular expression of green fluorescent protein, coupled with high-resolution in vivo videomicroscopy, to monitor steps in tumor metastasis. J Cell Sci 112:1835–1842
32. Farina KL, Wyckoff JB, Rivera J et al (1998) Cell motility of tumor cells visualized in living intact primary tumors using green fluorescent protein. Cancer Res 58:2528–2532
33. Condeelis J, Segall JE (2003) Intravital imaging of cell movement in tumors. Nature Rev Cancer 3:921–930
34. Wyckoff JB, Wang Y, Lin EY et al (2007) Direct visualization of macrophage-assisted tumor cell intravasation in mammary tumors. Cancer Res 67:2649–2656
35. Amoh Y, Li L, Yang M et al (2004) Nascent blood vessels in the skin arise from nestin-expressing hair follicle cells. Proc Natl Acad Sci USA 101:13291–13295
36. Amoh Y, Li L, Yang M et al (2005) Hair-follicle-derived blood vessels vascularize tumors in skin and are inhibited by doxorubicin. Cancer Res 65:2337–2343

37. Brown EB, Campbell RB, Tsuzuki Y et al (2001) In vivo measurement of gene expression, angiogenesis and physicological function in tumors using multiphoton laser scanning microscopy. Nat Med 7:864–868
38. Denk W, Strickler JH, Webb WW (1990) Two-photon laser scanning fluorescence microscopy. Science 248:73–76
39. Fukumura D, Yuan F, Monsky WL et al (1997) Effect of host microenvironment on the microcirculation of human colon adenocarcinoma. Am J Pathol 151:679–688
40. Fukumura D, Xavier R, Sugiura T et al (1998) Tumor induction of VEGF promoter activity in stromal cells. Cell 94:715–725
41. Huang MS, Wang TJ, Liang CL et al (2002) Establishment of fluorescent lung carcinoma metastasis model and its real-time microscopic detection in SCID mice. Clin Exp Metastasis 19:359–368
42. Wyckoff JB, Jones JG, Condeelis JS, Segall JE (2000) A critical step in metastasis: in vivo analysis of intravasation at the primary tumor. Cancer Res 60:2504–2511
43. Chambers AF, Groom AC, MacDonald IC (2002) Dissemination and growth of cancer cells in metastatic sites. Nat Rev Cancer 2:563–572
44. Yamauchi K, Yang M, Jiang P et al (2005) Real-time in vivo dual-color imaging of intracapillary cancer cell and nucleus deformation and migration. Cancer Res 65:4246–4252
45. Yamauchi K, Yang M, Jiang P et al (2006) Development of real-time subcellular dynamic multicolor imaging of cancer cell trafficking in live mice with a variable-magnification whole-mouse imaging system. Cancer Res 66:4208–4214
46. Nathanson SD (2003) Insights into the mechanisms of lymph node metastasis. Cancer 98:413–423
47. Hoshida T, Isaka N, Hagendoorn J et al (2006) Imaging steps of lymphatic metastasis reveals that vascular endothelial growth factor-C increases metastasis by increasing delivery of cancer cells to lymph nodes: therapeutic implications. Cancer Res 66:8065–8075
48. Padera TP, Kadambi A, di Tomaso E et al (2002) Lymphatic metastasis in the absence of functional intratumor lymphatics. Science 296:1883–1886
49. Gunn MD, Kyuwa S, Tam C et al (1999) Mice lacking expression of secondary lymphoid organ chemokine have defects in lymphocyte homing and dendritic cell localization. J Exp Med 189:451–460
50. Hayashi K, Jiang P, Yamauchi K et al (2007) Real-time imaging of tumor-cell shedding and trafficking in lymphatic channels. Cancer Res 67:8223–8228
51. Yamamoto N, Yang M, Jiang P et al (2003) Determination of clonality of metastasis by cell-specific color-coded fluorescent-protein imaging. Cancer Res 63:7785–7790
52. Glinskii AB, Smith BA, Jiang P et al (2003) Viable circulating metastatic cells produced in orthotopic but not ectopic prostate cancer models. Cancer Res 63:4239–4243
53. Berezovskaya O, Schimmer AD, Glinskii AB et al (2005) Increased expression of apoptosis inhibitor protein XIAP contributes to anoikis resistance of circulating human prostate cancer metastasis precursor cells. Cancer Res 65:2378–2386
54. Glinsky GV, Glinskii AB, Berezovskaya O et al (2006) Dual-color-coded imaging of viable circulating prostate carcinoma cells reveals genetic exchange between tumor cells in vivo, contributing to highly metastatic phenotypes. Cell Cycle 5:191–197
55. Goldberg SF, Harms JF, Quon K et al (1999) Metastasis-suppressed C8161 melanoma cells arrest in lung but fail to proliferate. Clin Exp Metastasis 17:601–607
56. Goodison S, Kawai K, Hihara J et al (2003) Prolonged dormancy and site-specific growth potential of cancer cells spontaneously disseminated from non-metastatic breast tumors revealed by labeling with green fluorescent protein. Clin Cancer Res 9:3808–3814
57. Katz MH, Bouvet M, Takimoto S et al (2003) Selective anti-metastatic activity of cytosine analog CS-682 in a red fluorescent protein orthotopic model of pancreatic cancer. Cancer Res 63:5521–5525
58. Katz MH, Bouvet M, Takimoto S et al (2004) Survival efficacy of adjuvant cytosine-analogue CS-682 in a fluorescent orthotopic model of human pancreatic cancer. Cancer Res 64:1828–1833
59. Schmitt CA, Fridman JS, Yang M et al (2002) Dissecting p53 tumor suppressor functions in vivo. Cancer Cell 1:289–298
60. Schmitt CA, Fridman JS, Yang M et al (2002) Senescence program controlled by p53 and $p16^{INK4a}$ contributes to the outcome of cancer therapy. Cell 109:335–346
61. Ewald AJ, Brenot A, Duong M et al (2008) Collective epithelial migration and cell rearrangements drive mammary branching morphogenesis. Dev Cell 14:570–581
62. Sakaue-Sawano A, Kurokawa H, Morimura T et al (2008) Visualizing spatiotemporal dynamics of multicellular cell-cycle progression. Cell 132:487–498
63. Livet J, Weissman TA, Kang H et al (2007) Transgenic strategies for combinatorial expression of fluorescent proteins in the nervous system. Nature 450:56–62
64. Zhao H, Doyle TC, Coquoz O et al (2005) Emission spectra of bioluminescent reporters and interaction with mammalian tissue determine the sensitivity of detection in vivo. J Biomed Opt 10(4):41210